Enhanced Photocatalytic Activity and Magnetic Properties of CNTs/Sn-doped Co3O4 Nanocomposite

Mahdi Kazazi (mahdi.kazazi@gmail.com)
University of Malayer https://orcid.org/0000-0002-2928-2545
Mahdi Norouzi
University of Malayer
Banafsheh Moradi
University of Malayer

Original Research

Keywords: Nanocomposite, Carbon nanotubes, Sn-doped cobalt oxide, Photocatalysis, UV light, Visible light

Posted Date: February 8th, 2021

DOI: https://doi.org/10.21203/rs.3.rs-184292/v1

Version of Record: A version of this preprint was published at Optical and Quantum Electronics on March 16th, 2021. See the published version at https://doi.org/10.1007/s11082-021-02802-5.

Enhanced photocatalytic activity and magnetic properties of CNTs/Sn-doped Co_3O_4 nanocomposite

Mahdi Kazazi*, Mahdi Norouzi, Banafsheh Moradi

Department of Materials Engineering, Faculty of Engineering, Malayer University, Malayer, Iran

Abstract– Photocatalysis is a green technology which transforms available photon energy into useful chemical energy. The reaction mechanism is based on the ability to create electron-hole pairs under appropriate light. Semiconductors have attracted great attention in photocatalysts because of their high photosensitivity. Spinel–type cobalt oxide nanorods have been prepared by a simple hydrothermal method using cobalt nitrate as precursor. Sn-doped Co_3O_4 was composited with carbon nanotubes for better photocatalytic activity. An extensive characterization of the prepared samples was carried out using X-ray diffraction (XRD), field emission scanning electron microscopy (FESEM), energy dispersive X-ray spectroscopy (EDS), Fourier transform infrared spectroscopy (FTIR), Vibrating sample magnetometer (VSM) and UV–Visible absorption spectroscopy. The XRD results show the formation of Co_3O_4 phase with FCC structure, FESEM confirms the nanorods morphology of the cobalt oxide and the VSM taken at room temperature shows an antiferromagnetic behavior. The investigation of photocatalytic activity of Co_3O_4 based was done by methyl orange dye. At the end, the responsible mechanism of CNT/Sn-CO was discussed.

Keywords– Nanocomposite, Carbon nanotubes, Sn-doped cobalt oxide, Photocatalysis, UV light, Visible light.

*Corresponding author. Tel.: +98 9183535611; fax: +98 8133339880.
E-mail addresses: m_kazazi@malayeru.ac.ir, mahdi.kazazi@gmail.com (M. Kazazi).

1. Introduction

Environmental water pollutions originated from the organic dye compound used in paint, leather, pigments, rubber, textile industries, and household chemicals are a threat to human health, which make allergy, cancer, skin discomfort, illness of kidneys, liver and reproductive system. Methyl orange (MO) is an azo dye that is used widely in textile, printing, pharmaceutical, and research laboratories. That's why; MO was favorited as a pollution model for photocatalytic decolorization in this work. Several ways have been studied to delete dyes or some pollution from water and industrial wastewater containing conventional coagulation, adsorption, chemical precipitation, reverses osmosis, ion exchange, filtering, and photocatalytic activity. Among the various techniques for the removal of dyes, adsorption and photocatalytic degradation are recommended as environmentally, cheap and efficient methods. However, although adsorption by low-cost materials is efficient for dye removal, this method produces a lot of solid wastes. Among the proposed methods for dye degradation, advanced oxidation processes or the same photocatalytic activity based on semiconductors or metal oxides are introduced as an effective method [1-5]. Semiconductors used in photocatalysis need to have certain properties like appropriate band gap energies, stability toward photo-corrosion, low cost, and nontoxic nature. Nano-sized semiconductor particles can possess enhanced photo-redox chemistries and reduction reactions that might not occur using coarse materials. This is due to the more available surface active sites and enhanced interfacial charge-carrier transfer rates in nano-sized materials, leading to their improved photocatalytic process. The photocatalytic properties of semiconductor materials depend mainly on their phase composition, doping, particle size, surface area, and morphology [6-

7]. In photocatalytic process, semiconductors especial metal oxides are activated with absorbing light such as UV light, visible light or both of them like sun light, the light is so important in this reaction because the energy of photons should be equal to or more than band gap (the band gap is characteristic for the electronic structure of materials and it (E_g) is the distance between the valence band of electrons and the conduction band and the Fermi level is located in it). After light absorption, the electrons in valence band (VB) vamoose into the conduction band (CB), that cause a charge separation process with the forming of positive holes in VB and negative electrons in CB. The electrons produced in CB could be trapped by O_2 and operate the formation of very reactive superoxide radical ion ($^{\bullet}O_2^-$) also the holes generated in VB react with molecules of water or hydroxide ions (OH^-) producing hydroxyl radicals ($^{\bullet}OH$). Finally the organic molecules could be oxidized to produce water and carbon dioxide [8-10]. Some parameters are important in photocatalytic process: the type of the photocatalytic semiconductor (n-type or p-type), the type of band gap of semiconductor (direct or indirect), the separation of electron-hole pair (composite or doping), the pH of the target solution (potential zeta of semiconductor), the temperature of solution (some of electrons and holes are recombination), and the light radiation used. According to the sun's light are containing small fraction of UV light (5%) and more fraction of visible light (45%). Therefore, one goal to improve performance of semiconductor nanocatalysts is to shift their response start from the UV region to the visible region. There are several ways to arrive this goal like doping, sensitizing and coupling [11-12].

Tricobalt tetraoxide (Co_3O_4) is an important antiferromagnetic in magnetic materials and shows p-type semiconductor in conducting property. Indeed cobalt oxide (Co_3O_4) is a complex of two valence of Co (Co^{2+} and Co^{3+}) with oxygen (O^{2-}) that are CoO and Co_2O_3. There is a variety of technological applications for cobaltite spinel such as gas-sensing, catalytic and electrochemical

ones, sensors, electrochromic devices, heterogeneous catalysts, and lithium batteries. Co_3O_4 with cubic normal spinel structure can be expressed as AB_2O_4 where A and B define the magnetic Co^{2+} ions in tetrahedral sites and non-magnetic Co^{3+} ions in octahedral sites. Co^{2+} ions have a high-spin state (S=3/2) while Co^{3+} ions possess a low-spin state (S=0) [13-15].

Carbon nanotubes (CNTs) are rolled-up sheets of layer carbon atoms (graphene) and they can be single-walled (SWCNT) or multi-walled (MWCNT). The rotation direction (chiral vector) of the graphene layers defines the electrical properties of the CNTs: perfect conductivity, semi-conductor, and, non-conducting. CNTs have many attentions because of their intrinsic mechanical, electrical, and thermal features, causing them appropriate for various applications such as transistors, electrical storage devices, and nanoscale machines. As a beneficial way to reduce the electron–hole recombination rate, increase the effective surface, and decrease the aggregation of semiconductors, various works have investigated the benefit of coupling of metal oxides or semiconductors to carbon materials like graphene oxide, carbon nanotubes, reduced graphene oxide, and carbon fibers. [8, 16]. Compared to pure metal oxides, many linked systems, such as SnO_2–CNT [17], TiO_2-CNT [18], and TiO_2–GO [19] show high photocatalytic activities by decreasing the recombination rate.

In this work, we synthesized CNT/Sn-Co_3O_4 nanocomposite by hydrothermal method. The effect of Sn doping and CNT additive on photocatalytic activity of cobaltite spinel were investigated. The structural, optical, and magnetic properties and photocatalytic action of the samples were investigated by XRD, VSM, FE-SEM, EDS and UV-visible analyses.

2. Experimental

2.1. Materials and method

Cobalt nitrate hexahydrate ($Co(NO_3)_2.6H_2O$), ammonium fluoride (NH_4F) and urea (CH_4N_2O) were used as precursors of cobalt oxide. In addition to the above materials, tin chloride dehydrate ($SnCl_2.2H_2O$) and carbon nanotubes multi-walled (CNTs 95 % purity, USnano) were used as precursors of Sn-doped Co_3O_4 and nanocomposite respectively. Hydrothermal issue is one of the most generally used methods for synthesis of nanomaterials. It is a great technology for crystal growth and to control the morphology with useful properties. In this study, three samples were prepared by hydrothermal route.

2.2. Synthesis of Co_3O_4 nanorod

For the synthesis of pure cobalt oxide, the mixture prepared with 2.25 mmol of cobalt nitrate hexahydrate, 3 mmol of ammonium fluoride and 15 mmol of urea in 40 mL distilled water were stirred (30 min) at room temperature and then poured to a 50 mL Teflon-lined autoclave and heated at 120 °C (4 h) for the hydrothermal process. In order to get pure cobalt oxide, after the solution was cooled, it was centrifuged and washed, then dried at 60 °C for 12 h. Finally, the dried precipitate was calcined at 300 °C for 2 h and the black powder was obtained [20].

2.3. Synthesis of Sn-doped Co_3O_4

To synthesize the Sn-doped Co_3O_4 sample, the quantity of above (or Co_3O_4) precursors were calculated and also adding the right amount of $SnCl_2.2H_2O$. In the next step, all precursors dissolved in 40 mL of distilled water respectively and the solution was stirred for 30 min and using ultrasonic for 10 min. then, the solution was poured into Teflon-lined stainless steel autoclave and was heated at 120 °C for 4 h. After terminating the reaction, the obtained powder was filtered and washed with water several times. In the last step, the dried powders were calcined at 300 °C for 2 h, quite similar to the previous one.

2.4. Synthesis of CNT/Sn-Co_3O_4 nanocomposite

To eliminate the catalysts of CNTs were stirred in a mixture of $[H_2SO_4]/[HNO_3]$ (3:1) at 60 °C for 6 h. After that, the CNTs were washed with ethanol distilled water several times by centrifugation and drying at 70 °C in oven. The 0.015 g of as-prepared CNTs powders were dispersed in 40 ml of distilled water in an ultrasonic bath. Then the calculated quantity of $Co(NO_3)_2.6H_2O$ and $SnCl_2.2H_2O$ and NH_4F and CH_4N_2O were added to it and transferred to a Teflon-lined stainless steel autoclave and was heated at 120 °C for 4 h. Finally, the as-obtained powders were calcined at 300 °C for 2 h. The schematic illustration of the CNT/Sn-Co_3O_4 nanocomposite preparation is presented in Fig. 1.

2.5. Characterization of the samples

The samples based on cobalt oxide were characterized in various terms. Crystal structure and Phase identification of the powders were examined by X-ray diffraction (XRD, Uni-santis

XMD-300). The morphology of the samples was obtained by field emission scanning electron microscopy (FESEM, Mira 3-XMU). Energy dispersive X-ray spectroscopy (EDS) is an analytical technique used for the elemental analysis or chemical characterization of samples. IR spectra, in the range of 400-4000 cm^{-1}, were recorded in KBr pellets using a Perkin-Elmer FT-IR spectrophotometer at room temperature. Vibrating sample magnetometer (VSM, Meghnatis Kavir Kashan Co., Iran) was used to study the magnetic property of the products.

2.6. Photocatalytic measurements

We dispersed 0.001 g of synthesized Co_3O_4 nanorods separately in 10 ml of ethanol by the ultrasonic bath for calculating the band gap. A UV-Vis spectrophotometer was used to record the absorption spectra of the samples in the range of 400–800 nm, then, by drawing the Tauc plot the optical bandgap was determined. For investigation of photocatalytic activity of samples the Methyl Orange (MO) molecule was selected as a model pollutant (30 ppm). 0.1 g of Co_3O_4-based photocatalyst material was added into a beaker (25 ml) containing 10 mL of MO aqueous solution. Prior to irradiation, for checking the absorption-disabsorption of MO molecule on the surface of the photocatalysts, the MO solution containing photocatalyst powders was stirred for 5 min in the dark box. Because of the porous structure of Co_3O_4 nanorods as photocatalyst, some of MO molecule was absorbed, but when increased the time of absorption, the amount of absorption characteristic was constant. The material at this condition was used for photocatalytic activity measurements and cycling stability. After investigate the amount of absorption, radiation was carried out by 125 Watts UV lamp and also 100 Watts visible-light lamp 5 cm above the beaker. In all experiments, the irradiation distance and rotational speed of stirrer were fixed. At certain timeouts

(5, 10 and 15 min), about 5 mL suspension was collected and MO solution was separated from samples by centrifugation. The decolorization of MO was monitored by measuring the absorbance by UV-Visible spectrometry.

3. Results and discussion

3.1. **Characterization of cobaltite based samples**

The XRD patterns of the Sn-doped CO and CNT/Sn-CO nanocomposites as well as pure CO are shown in Fig. 2. Also, sharp peaks of the Co_3O_4 show crystalline structure of synthesis particles and all diffraction peaks in XRD spectrum of the samples are in match with JCPDS card (No. 01-080-1542) associated with face-centered cubic (fcc) phase of Co_3O_4 (space group: Fd-3m). The synthesis samples are completely pure because reflection peaks for other impurities aren't observed. The diffraction peaks at 28.36°, 47.14°, 55.89°, 68.82°, and 94.51° can be respectively denoted as (111), (220), (311), (400), and (440). The crystal structure of Co_3O_4 is in normal spinel and the Co^{3+} and Co^{2+} ions are surrounded by six and four oxygen atoms, respectively. Scherrer's equation: is a formula that reports the size of micrometre crystallites in a solid by a diffraction pattern, $D(nm) = \frac{0.9\,\lambda}{\beta \cos\theta}$ where D is the mean size of the domains, λ is the X-ray wavelength (λCu=1.54 A°), β is the broadening at half the maximum intensity (FWHM), and θ diffraction angle of the peak. The average crystallite sizes of the CO and Sn-CO determined by applying equation to the maximum intensity peak of XRD pattern at 2θ ≅55.8° are about 15.4 and 12.7 nm, respectively.

FESEM images of the CO, Sn-CO, and CNT/Sn-CO samples are shown in Fig. 3 at different magnifications. Three-dimensional nanorods-shaped Co_3O_4 were formed by hydrothermal synthesis without added surfactant and ligands. As can be seen, images with more magnification show that the all nanorods including many small nanoparticles, which they are next to each other for creating porous nanorods. Their diameter and length of nanorods could be tuned by change the annealing temperature and time. After doping of Sn in Co_3O_4, some of nanorods stick to each other and shape some of Co_3O_4 nanoplates (Fig. 3 c,d). Moreover, FESEM images of the CNT/Sn-CO nanocomposite synthesized are shown in Fig.3e and f. the surface of Sn-CO coated with the CNTs for better photocatalytic activity. It is clear that the CNT/Sn-CO nanocomposites are susceptible to yield powders in irregular shape and with non-uniform particle size, because of blending of three forms of nanoparticles: nanorods, nanoplates, nanotubes.

EDX spectra of the prepared CO, Sn-CO, and CNT/Sn-CO nanocomposites are shown in Fig. 4 a, b, and c respectively. The spectrum of CO shows only the peaks of cobalt and oxygen without any another peak of other elements that were in synthesis. Each element has a unique atomic structure allowing a unique set of peaks on its electromagnetic emission spectrum, hence in EDS spectra EDS spectra can be used for the type of elements and also the concentration of each element of the prepared. EDS spectrum related to Sn-CO sample shows only cobalt, oxygen, and tin peaks without impurity peak. Fig. 4 c show EDX spectrum of CNT/Sn-CO included peaks related to the C, Co, and Sn elements. Further, the atomic ratio of Co, C, and Sn was found to be 28.73, 18.26, and 7.10 respectively, that confirmed the presence of tin and carbon nanotube only indicating the synthesized material. Corresponded to EDS mapping images illustrated in Fig. 5, Co, Sn, and C are distributed evenly throughout the whole area of the CNT/Sn-CO nanocomposite.

The functional groups of Co_3O_4, Sn-Co_3O_4, and CNT/Sn-CO composites were studied by FTIR spectra as shown in Fig. 6. In three samples, two bands appeared at 3380.3 cm^{-1} and 1600 cm^{-1} responsible for O-H band and CO_2 absorb from the environment that usually happens in nanostructure materials due to its high surface. The Co_3O_4 spectrum exhibits two main peaks at 561.1cm^{-1} and 660.8 cm^{-1} refer to the (Co–O) modes of Co_3O_4 spinel oxide. Observed results in this work well agree with other research groups. [21]. In the spectrum of the Sn-CO, the characteristic peaks of oxygen-metal are occurred at 660 cm^{-1} and 561 cm^{-1} that are related to the stretching and bending modes of the Co-O and Sn-O bonds. In the CNT coated Sn-CO, the characteristic peaks of Co_3O_4 are appeared in the same regions and a peak at 1625 cm^{-1} is attributed to C=C bond in MWCNTs and the band at about 1100 cm^{-1} is related to C–C bonds.

3.2. Magnetic properties

The most common way to show the magnetic properties of a material is by a plot of magnetization M for various applied magnetic field that named hysteresis loops. The hysteresis loops of samples are shown in Fig. 7. The coercivity, remanence and saturation magnetization of the CO, Sn-CO, and CNT coated Sn-CO samples are summarized in Table 1. The magnetic induction can be decreased to zero by using a reverse magnetic field and this field is known as the coercivity (H_c). When the applied magnetic field is reduced to zero, the remaining magnetization is named the remanent magnetization (M_r). When the applied magnetic field is increased, the magnetic dipoles of material are aligned in the field direction, which is named saturation magnetization (M_s). According to hysteresis loops, all samples show antiferromagnetic behavior,

whereas remanences of the samples are nearly zero and saturation magnetization in Sn-CO sample is decreased because of sitting Sn atoms instead of Co^{2+} ions in tetrahedral sites. By magnetic measurements we notice a favorite result that is increase in saturation magnetization of the CNT/Sn-CO compared with the CO and Sn-CO due to the magnetic properties of CNTs related to the magnetic catalyst material that remaining inside carbon nanotubes after the synthesis procedure [22].

3.3. Photocatalytic behavior

3.3.1. Band gap calculation

It's clear that photocatalytic activity of nanomaterials depends on their optical property and shape of those. The optical property of the two samples was investigated by an UV–Visible spectrophotometer. Fig.8a illustrates the UV–Vis spectra of the CO and Sn–CO samples in the wavelength range of 400–800 nm. In this study, a Tauc plot is used to calculate the optical band gap energies of the Sn–doped Co_3O_4 samples, Tauc plot shows the quantity versus the photon energy (hυ) on the horizontal axis and the quantity $(\alpha h\upsilon)^n$ on the vertical axis, according to equation: $(\alpha h\upsilon)^n = A\left(h\upsilon - E_g\right)$, where h is Planck's constant, A is a constant, υ is the frequency and α is an absorption coefficient [23]. (n=1/2 for indirect band gap of the semiconductor and n=2 for direct band gap). The Co_3O_4 has a direct band gap material because its valence-band maxima and conduction-band minima are both located at the X point [13]. According to equation, the band gap of the samples can be approximated as shown in Fig. 8b. The edge position of the valence

band (VB) and conduction band (CB) for the Co_3O_4 can be determined using the following equations [24]:

$$E_{VB} = \chi - E_e + (0.5)E_g (1)$$

$$E_{CB} = E_{VB} - E_g (2)$$

where χ is the absolute electronegativity of the semiconductor (the χ of Co_3O_4 is 5.93 [23]), E_e is the energy of free electrons on the hydrogen scale (4.5 eV) and E_g is the band gap of the semiconductor (2.56 eV). According to the top information, the edge position of VB (O 2p) and CB (Co 3d) was calculated to be 2.73 and 0.13 (eV), respectively. The electrons in the conduction band of Co_3O_4 cannot reduce more O_2 to yield $^{\bullet}O^-_2$ because the conduction band edge potential of Co_3O_4 is more than the standard redox potential (-0.39 eV). Thus, the proposed for solving this problem is doped Sn in Co_3O_4.

3.3.2. Photocatalytic activity

The photocatalytic performance of the three samples were measured with methyl orange (MO) dye. For the decrease in concentration of the MO by Co_3O_4-based particles, the MO solution was acidified (pH = 3). Before the photocatalytic degradation experiment, the MO solution and Co_3O_4 -based were stirred together for 5 min to check an adsorption-desorption in the dark at room temperature. Although the Co_3O_4 -based shows the nearly highest adsorption efficiency because of Co_3O_4 nanorods mesoporous, but the photocatalytic activity occur. The absorption spectra of MO by pure Co_3O_4 under UV light and visible light irradiation for various durations show in Fig. 9a and b. It can be seen that with increasing the exposure time the intensity of peak decreases. Fig.

9c and d show the UV–Vis absorbance spectra obtained for the MO degradation by Sn-Co_3O_4 under UV and visible light irradiation at different time intervals. The photocatalytic activity of Sn-CO is better than the pure CO, because of some state of Sn (5p orbital) located above the standard redox potential. Another reason of that is postpone the recombination electron and hole by new trap state of Sn in band gap. In order to improve the photocatalytic efficiency, the Sn-CO mixes with CNT. Fig. 9e shows the change in absorption spectra for the photocatalytic degradation of MO by CNT/Sn-CO nanocomposite under visible light. Stability and reusability of the CNT/Sn-CO nanocomposite photocatalysts are important factors that have an effect on their practical benefit. For evaluating the cycling stability, previously used CNT/Sn-CO nanocomposite was removed from the solution by centrifugation for 5 times. The obtained results of these works are demonstrated in Fig. 9f. Also, after 5 cycles, the collected powders were analyzed using XRD and it shows that the CNT/Sn-CO nanocomposite was not altered after photocatalytic activity experiments.

3.3.3. Photocatalytic mechanism

For better understanding photocatalyst activity, the mechanism of the CNT/Sn-CO under visible light can be schematically described in Fig. 10. Photocatalytic degradation include three steps: (a) Appropriate absorption of the MO molecules on the surface of semiconductor (nano size), (b) Proper light radiation for exciting, and (c) production the radicals for degradation by electrons and holes. As the Co_3O_4 is excited with photons having energy content equal to or more than the band gap, the electrons in (VB) are stimulated into the (CB), electron vacancies in valence

band is holes with positive charge. Some of generation electrons and holes are recombinant quickly before participate in photocatalyst reaction, therefore the lifetime of an electron hole pair is few nanoseconds. In this study, the lifetime of them increase by two method, Sn doping and CNT coated. The photogenerated hole and electron in band gap of Sn-CO are trapped in new trap state of Sn. When the Sn-CO in contact with CNTs, electron can migrate from the conducting band of CO to the CNTs surface because of the Fermi level of CNTs are lower than the conducting band of CO. Thus, CNTs accept and save photogenerated electrons and prevent the recombination of electrons and holes, resulting in a better photocatalytic activity.

The photocatalysis semiconductor is limited by a major phenomenon: nanosize particles in suspension are difficult to collect and pick up after their application in dye or wastewater. The advantages of CO is that collect by magnet in solution. Also, the semiconductor's element needs to have more than one stable valence state and not corrosion by holes form after photon radiation. Another benefit of CO is that exist two state Co^{2+} and Co^{3+}. Electrons can be holded easily by dissolved oxygen molecule in the MO solution, producing anion superoxide ($^{\bullet}O_2^-$) radicals. The generated holes in the valance band of Sn-CO easily oxidize OH^- to reactive hydroxyl ($^{\bullet}OH$) radicals. $^{\bullet}O_2^-$and $^{\bullet}OH$ could participate directly in the photocatalytic degradation reaction of MO, according to the following equations:

$$Co_3O_4 + h\upsilon \rightarrow e^- + h^+$$

$$Co^{3+} + e^- \rightarrow Co^{2+}$$

$$Co^{2+} + O_2 \rightarrow Co^{3+} + {}^{\bullet}O^-_2$$

$$h^+ + OH^- \rightarrow {}^{\bullet}OH$$

$$^{\bullet}O_2^- \text{ and } {}^{\bullet}OH + \text{Methyl Orange} \rightarrow H_2O + CO_2$$

Conclusion

In conclusion, cobalt oxide (CO), Sn-doped CO (Sn-CO) nanorods and CNT/Sn-CO nanocomposites were successfully synthesized by a hydrothermal method. Characterization of samples was performed by X-ray diffraction, Field emission scanning microscopy, energy dispersive X-ray spectroscopy, Fourier transform infrared spectroscopy, Vibrating sample magnetometer and UV–Visible absorption spectroscopy. The effect of Sn doped and carbon nanotube on photocatalytic activity and magnetic properties were investigated. Our studies show that the photocatalytic activity is better because of generated hole and electron. The recycling process was investigated for 5 times and displayed good stability with notices to photocatalytic activity, with less than 10% decreased from its primary activity during performance. Another results of this experimental also show that saturation magnetization of the Sn-CO is decreased but the saturation magnetization of CNT/Sn-CO is increased, due to the magnetic catalyst material that remaining inside carbon nanotubes after the synthesis procedure.

Acknowledgement

This work was financially supported by the Malayer University (Grant No.: 84/9-1-295).

References

[1] O.A. Yildirim, T. Ozturk, IntechOpen. Chapter 5(2017).

[2] D. Channei, B. Inceesungvorn, N. Wetchakun, S. Ukritnukun, A. Nattestad, J. Chen, S. Phanichphant,Sci. Rep. **4**, 5757 (2014).

[3] M. Shaban, A. M. Ashraf, M. R. Abukhadra, Sci. Rep. **8**, 781 (2018).

[4] M. Kazazi, B. Moradi, M. DelshadChermahini J. Mater. Sci. Mater. Electron. **30**, 6116 (2019).

[5] S. Abbasi, M. Hasanpour. J Mater Sci: Mater Electron.**2** (2017).

[6] R.M. Mohamed, D.L. McKinney, W.M. Sigmund, Mater. Sci. Eng. R Rep. **73**, 1(2012).

[7] S. Suresh. J NANOSCI NANOTECHNO. **3**: 62 (2013).

[8] T. A. Sale. IntechOpen . Chapter 21. (2013).

[9] J. You, Y. Guo, R. Guo, X. Liu. Chem. Eng. **373**, 624 (2019).

[10] A. Gnanaprakasam, V.M. Sivakumar, M. Thirumarimurugan. INDIAN J ENG MATER S. 16 pages (2015).

[11] C. Xu, P. R. Anusuyadevi C. Aymonier, R. Luque, S. Marre. Chem.Soc. Rev. **48**, 3868 (2019).

[12] S. Demirci, T. Dikici, M. Yurddaskal, S. Gultekin, M.Toparli, E. Celik,Appl. Surf.Sci.**390**, 591 (2016).

[13] A.F.Lima. J. Phys. Chem. Solids. **75**. 148 (2014).

[14] J.M. Xu, J.P. Cheng. J. Alloys Compd. **686**. 753 (2016).

[15] X. R. Zhao, Y.Q. Cao, J. Chen, L. Zhu, X. Qian, A.D. Li, D. Wu. Nanoscale Res. Lett.**12**. 497 (2017).

[16] A. Alwash, H. Adil, Z. Hussain, E. Yousif. ANOAJ. **1**. 3 (2018).

[17] S. P. Kima, M.Y. Choib, H. C. Choia. Appl. Surf. Sci. **357**. 302 (2015).

[18] M. Shaban, A. M. Ashraf, M.R. Abukhadra. Sci. Rep. **8**. 781 (2018).

[19] S.P. Kim, H. C. Choi. Bull. Korean Chem. Soc. **35**. 9 (2014).

[20] M. Kazazi, R. Karami. Solid State Ion. **308**. 8 (2017).

[21] S. Dubey, J. Kumar, A. Kumar, Y. C. Sharma. ADV POWDER TECHNOL. **29**. 8 (2018).

[22] K. Lipert, M. Ritschel, A. Leonhardt, Y. Krupskaya, B. Buchner, R. Klingeler. J. Phys.: Conf. Ser. **200**. (2010).

[23] S. Baia, H. Liua, R. Luoa, A. Chena, D. Lia. RSC Adv. **4**, 62862 (2014).

[24] M.J. Islam, D.A. Reddy, J. Choi, T.K. Kim, RSC Adv. **6**, 19341 (2016).

Figure captions

Fig. 1. Schematic representation of preparing steps of the CNT/Sn-CO sample.

Fig. 2. XRD patterns of the as-synthesized Co_3O_4-based samples.

Fig. 3. FESEM images of the as-prepared (a, b) CO, (c, d) Sn-CO and (e, f) CNT/Sn-CO samples at various magnifications.

Fig. 4. EDS spectra of the as-prepared (a) CO, (b) Sn-CO and (c) Ag/Sn-CO samples.

Fig. 5. FESEM image of CNT/Sn-CO nanocomposite with corresponding EDS maps for (a) Co, (b) Sn, and (c) C elements.

Fig. 6. FT-IR spectra of the CO, Sn-CO, and CNT/Sn-CO samples.

Fig. 7. Magnetization curves of the CO, Sn-CO, and CNT/Sn-CO samples at room temperature. The inset shows a magnified view of the central region of loops.

Fig. 8. (a) UV–Vis spectra of the CO and Sn-CO samples; (b) Schuster-Kubelka-Munk absorption function of CO and Sn-CO samples versus photon energy.

Fig. 9. Change in the absorption spectra of methyl orange by CO under (a) UV light and (b) Visible light, Sn-CO under (c) UV light and (d) Visible light, CNT/Sn-CO under (e) Visible light; (f) Cycling runs of MO decolourisation by CNT/Sn-CO samples.

Fig. 10. A model for the photocatalytic mechanism of CNT/Sn-CO nanocomposite.

Table1. The magnetic parameters (coercivity (H_c), saturation magnetization (M_s) and remanence (M_r)) of the CO, Sn-CO, and CNT/Sn-CO samples.

Sample	**H_c (Oe)**	**M_s (emu/g)**	**M_r (emu/g)**
CO	710.203	1.026	-0.049
Sn-CO	151.010	0.573	-0.002
CNT/Sn-CO	-303.332	1.103	0.047

Figures

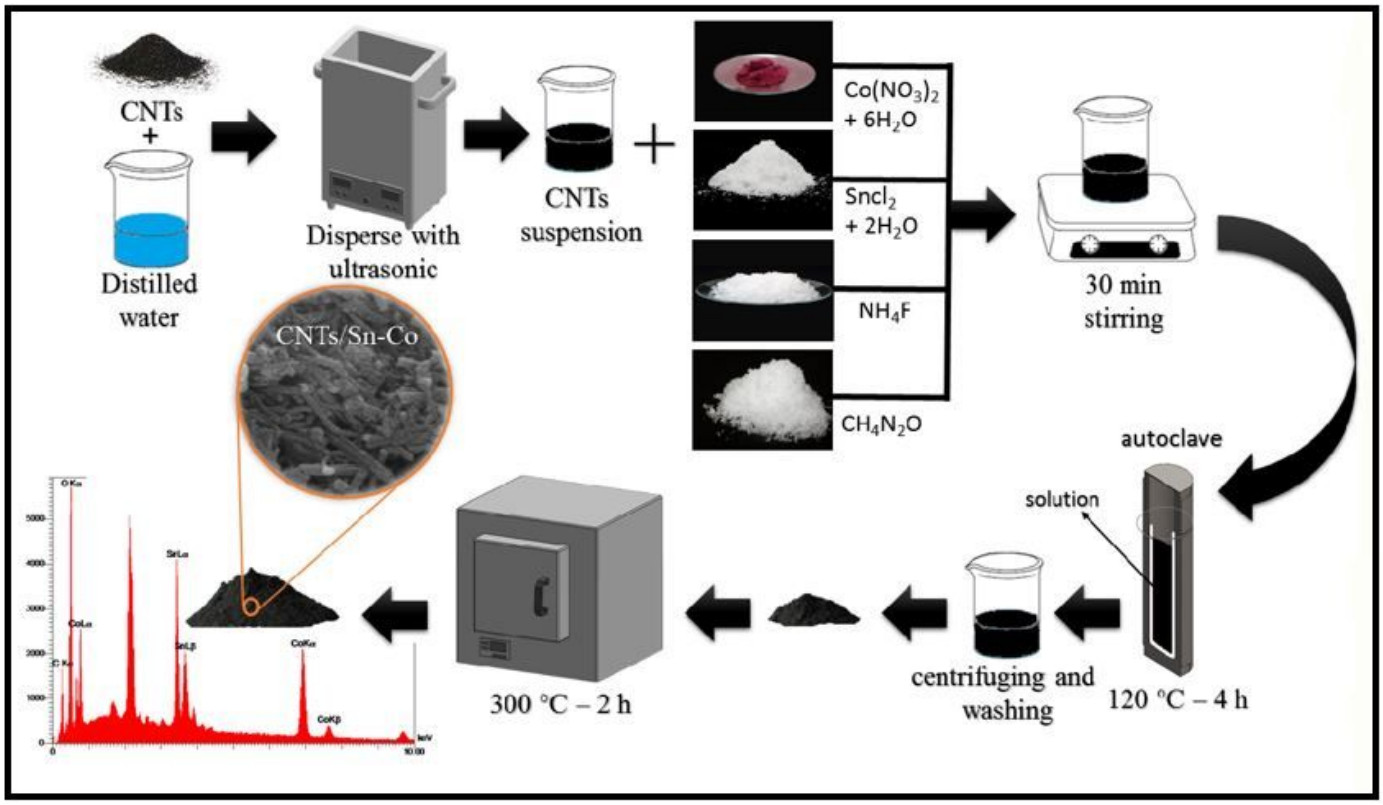

Figure 1

Schematic representation of preparing steps of the CNT/Sn-CO sample.

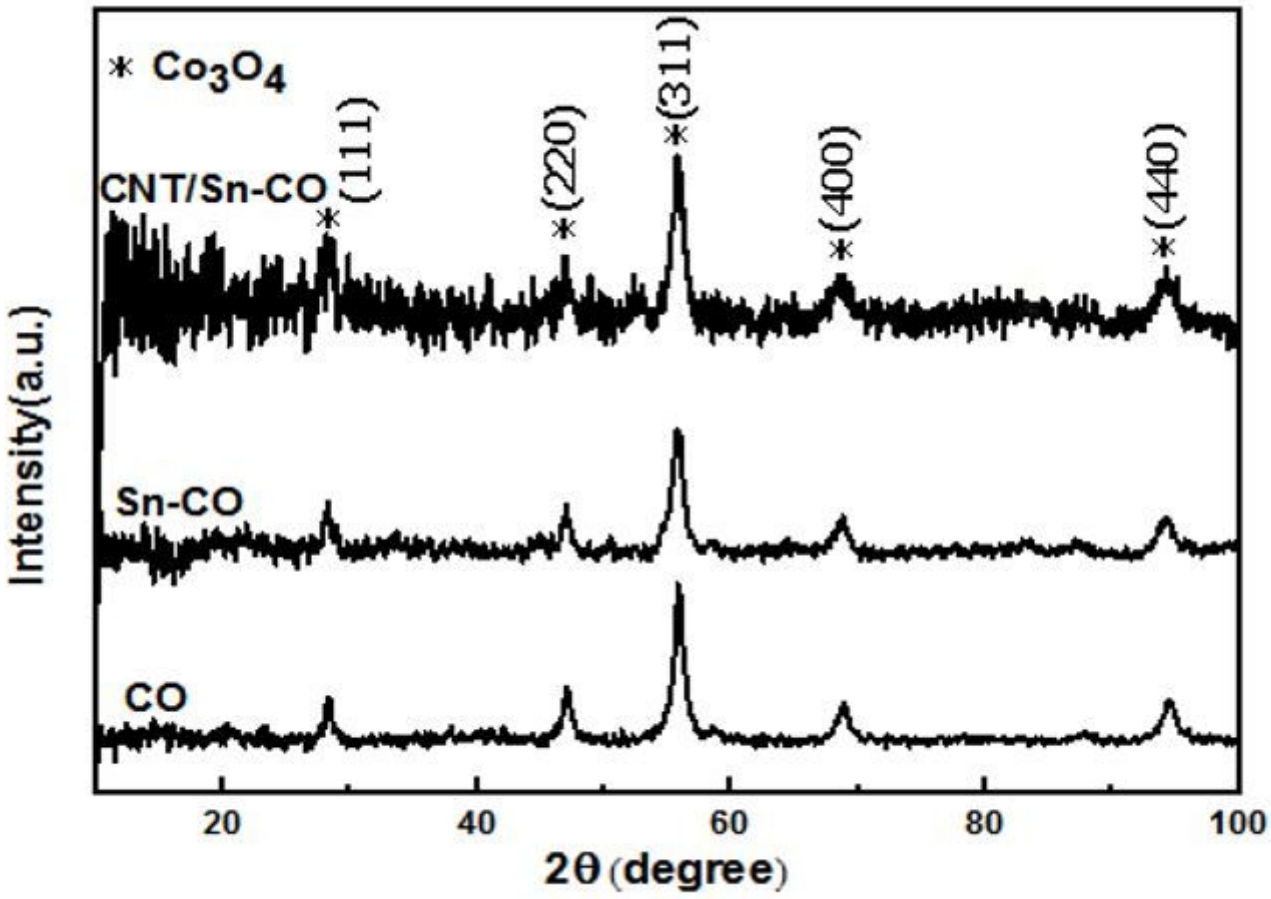

Figure 2

XRD patterns of the as-synthesized Co3O4-based samples.

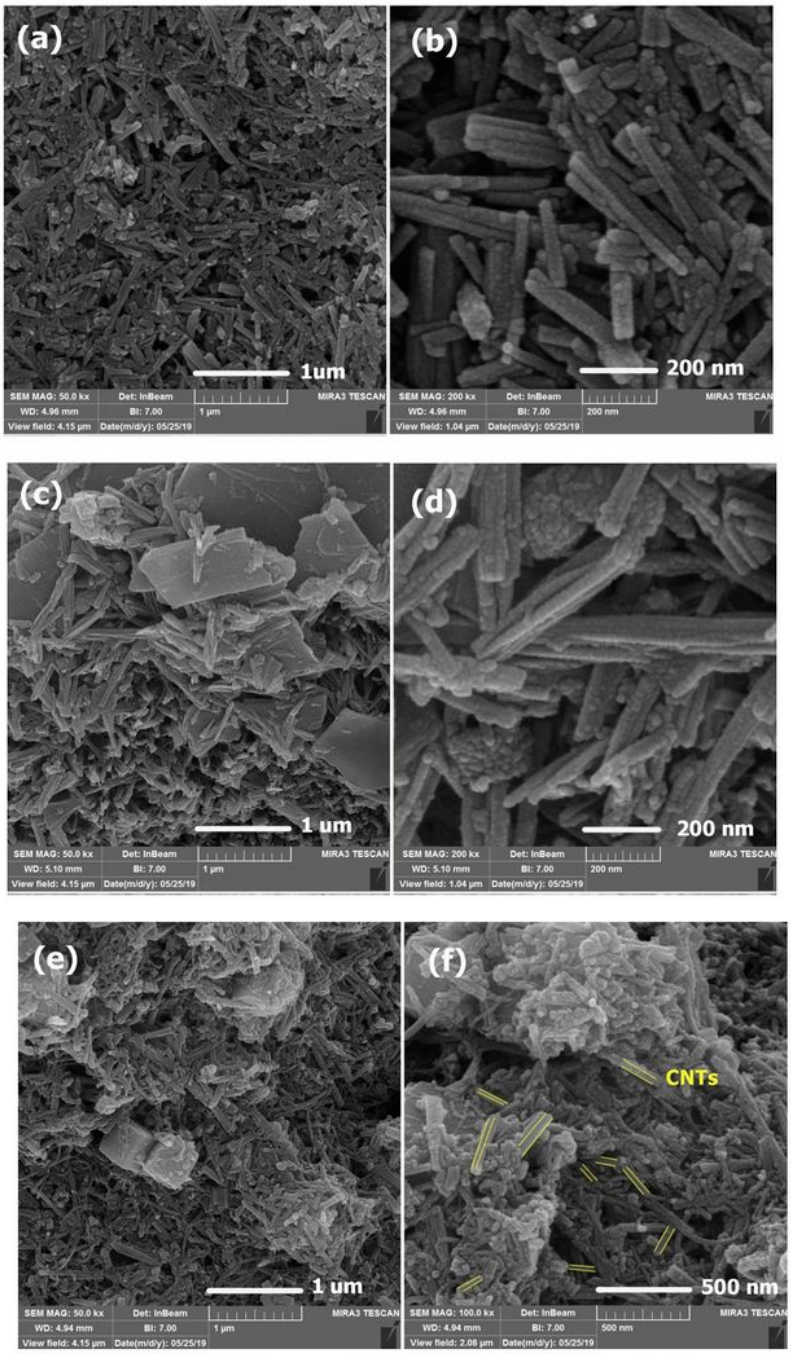

Figure 3

FESEM images of the as-prepared (a, b) CO, (c, d) Sn-CO and (e, f) CNT/Sn-CO samples at various magnifications.

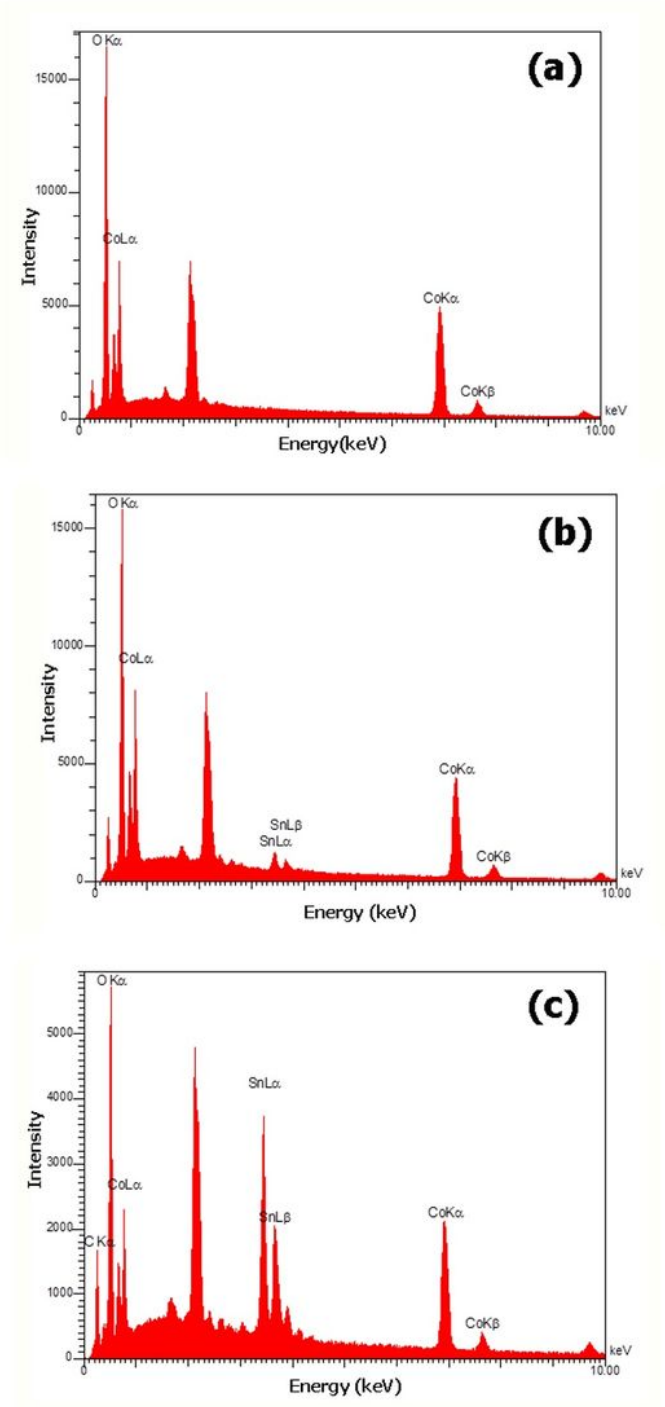

Figure 4

EDS spectra of the as-prepared (a) CO, (b) Sn-CO and (c) Ag/Sn-CO samples.

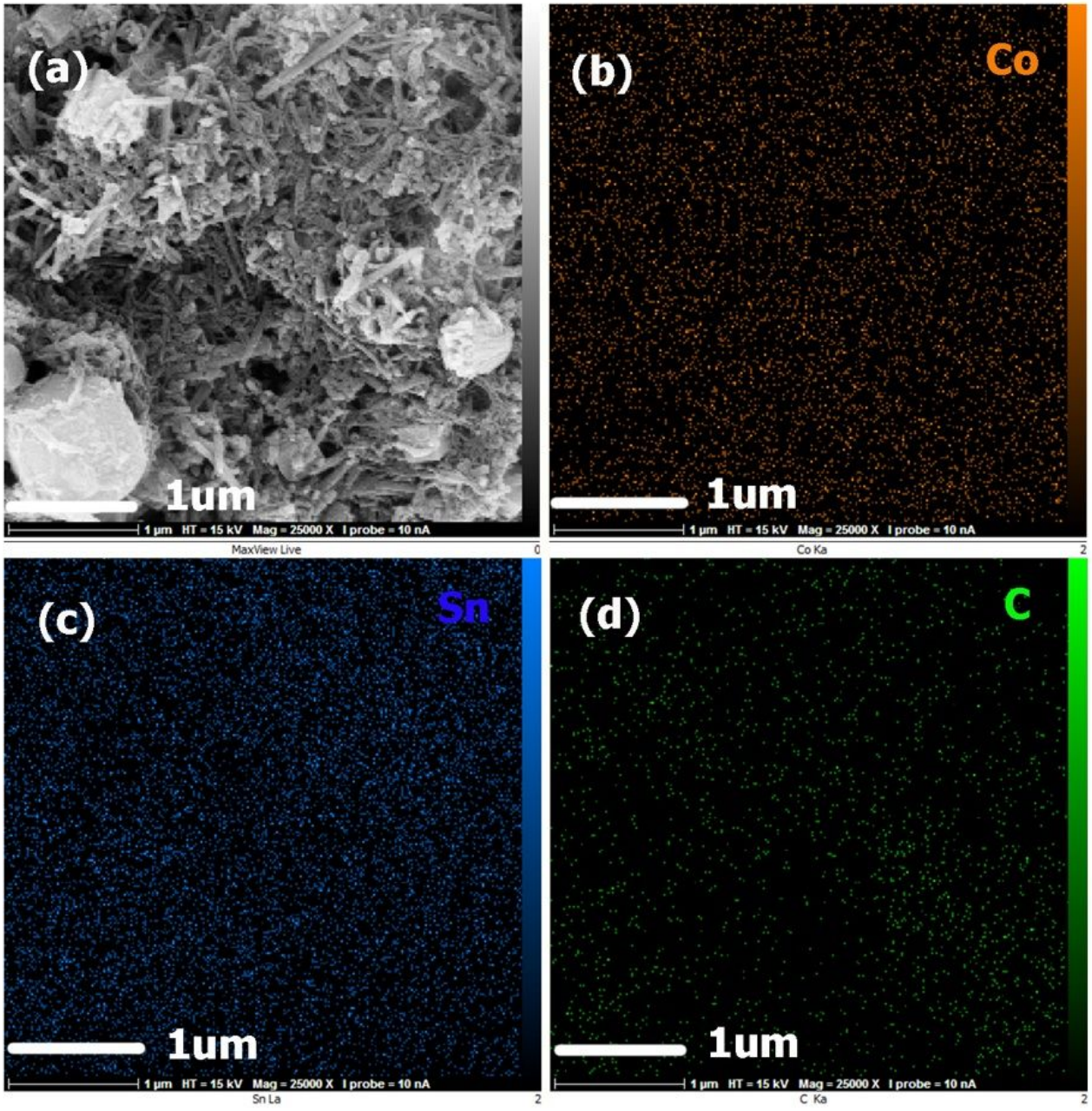

Figure 5

FESEM image of CNT/Sn-CO nanocomposite with corresponding EDS maps for (a) Co, (b) Sn, and (c) C elements.

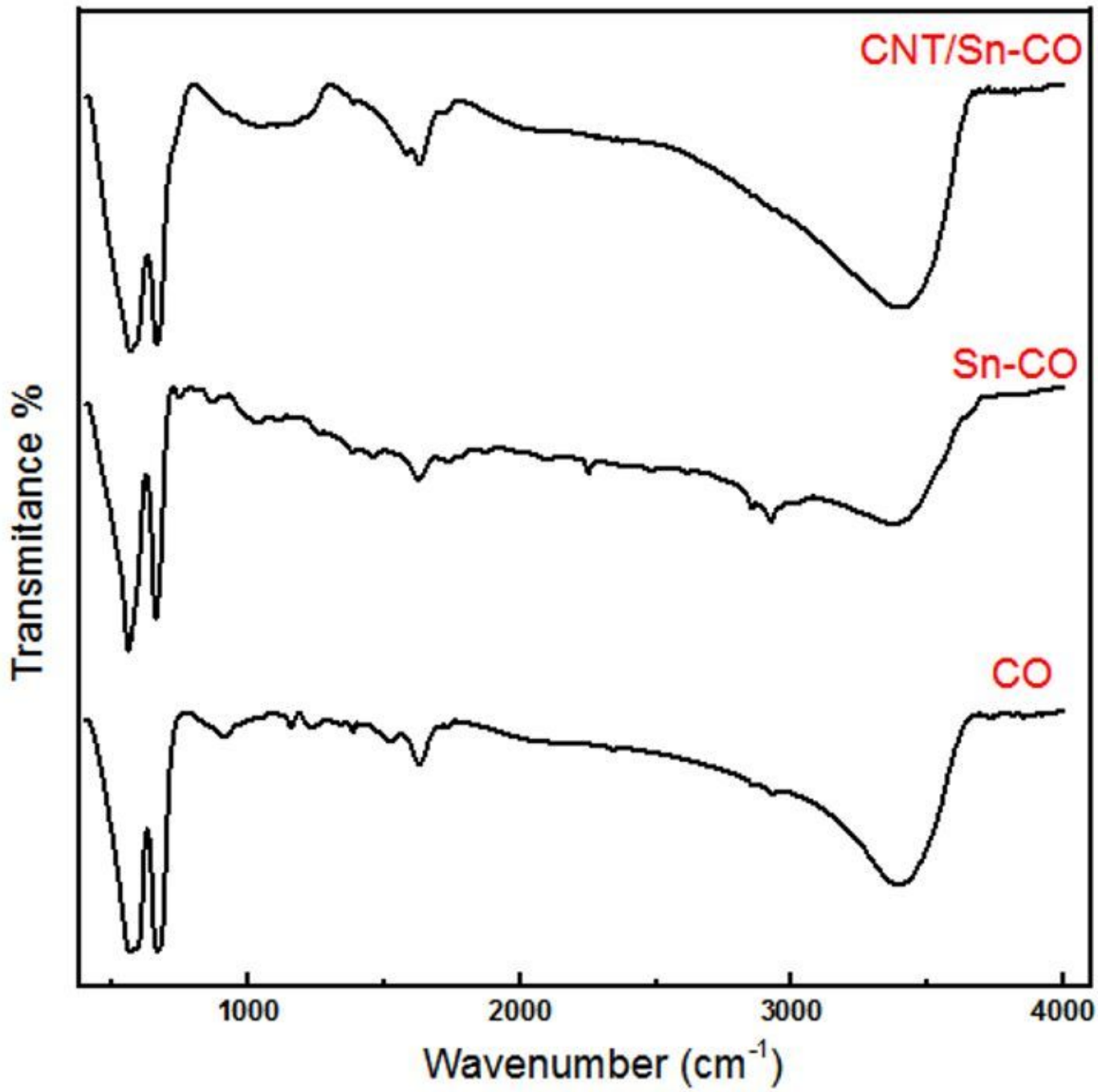

Figure 6

FT-IR spectra of the CO, Sn-CO, and CNT/Sn-CO samples.

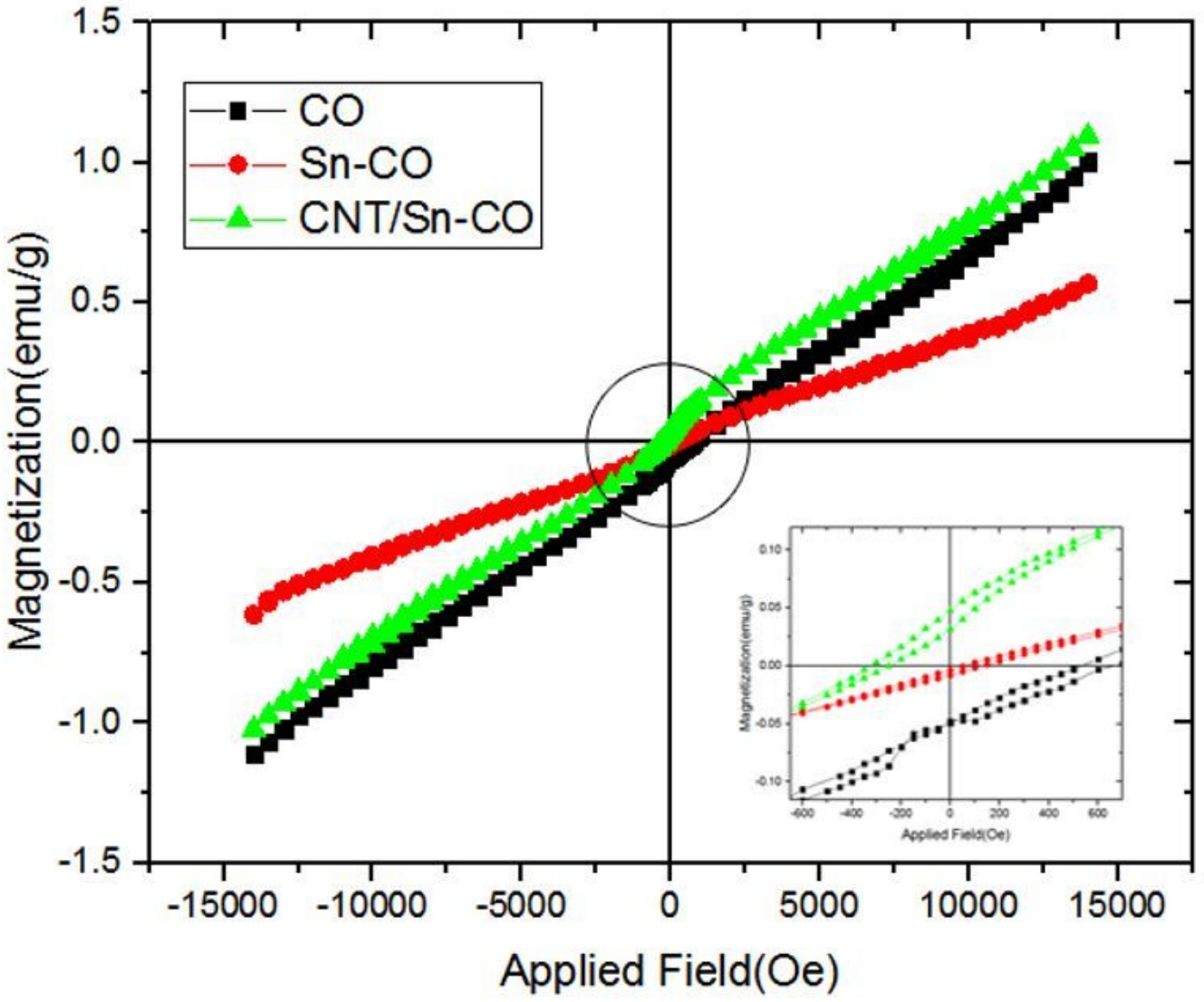

Figure 7

Magnetization curves of the CO, Sn-CO, and CNT/Sn-CO samples at room temperature. The inset shows a magnified view of the central region of loops.

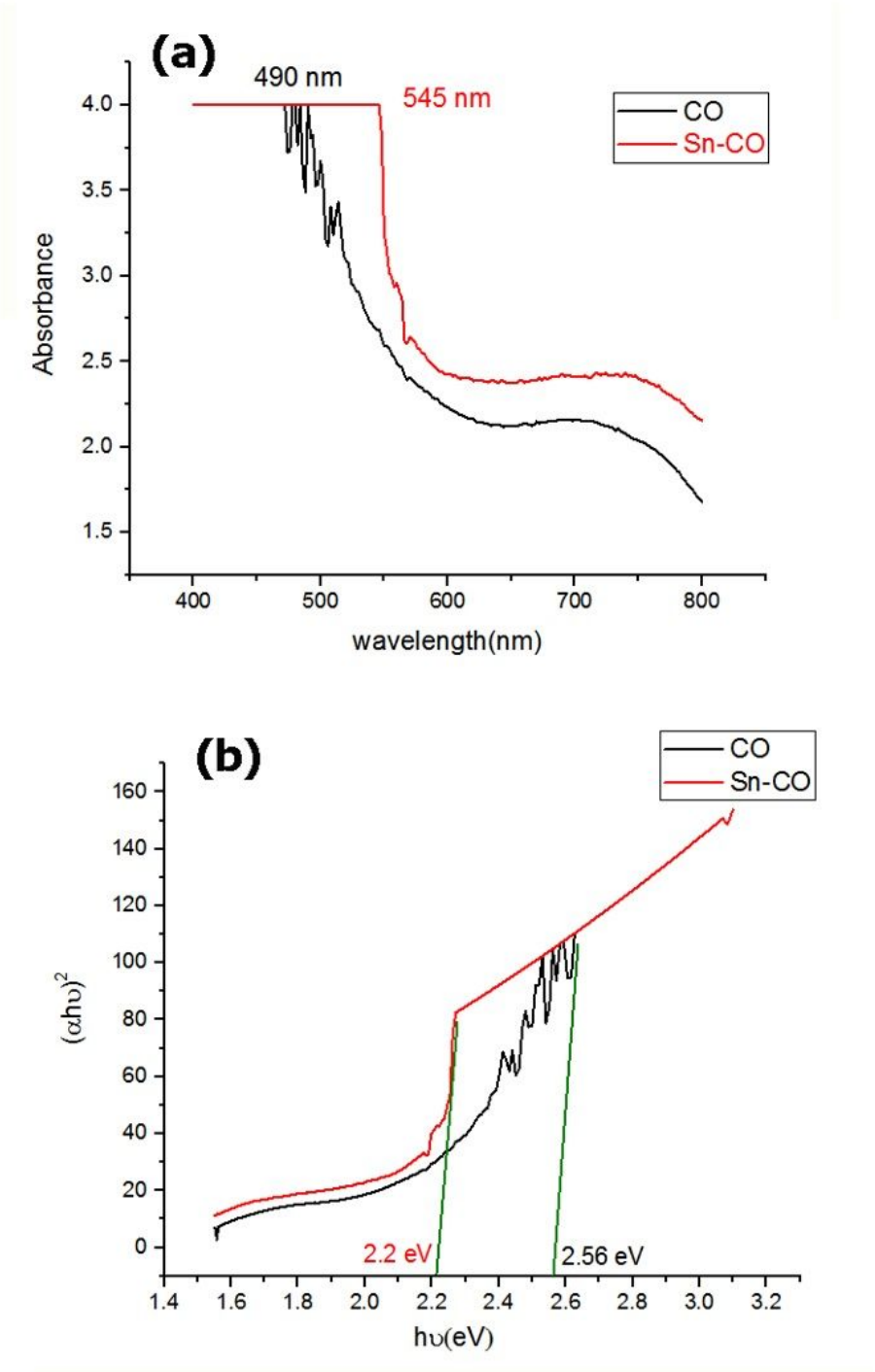

Figure 8

(a) UV–Vis spectra of the CO and Sn-CO samples; (b) Schuster-Kubelka-Munk absorption function of CO and Sn-CO samples versus photon energy.

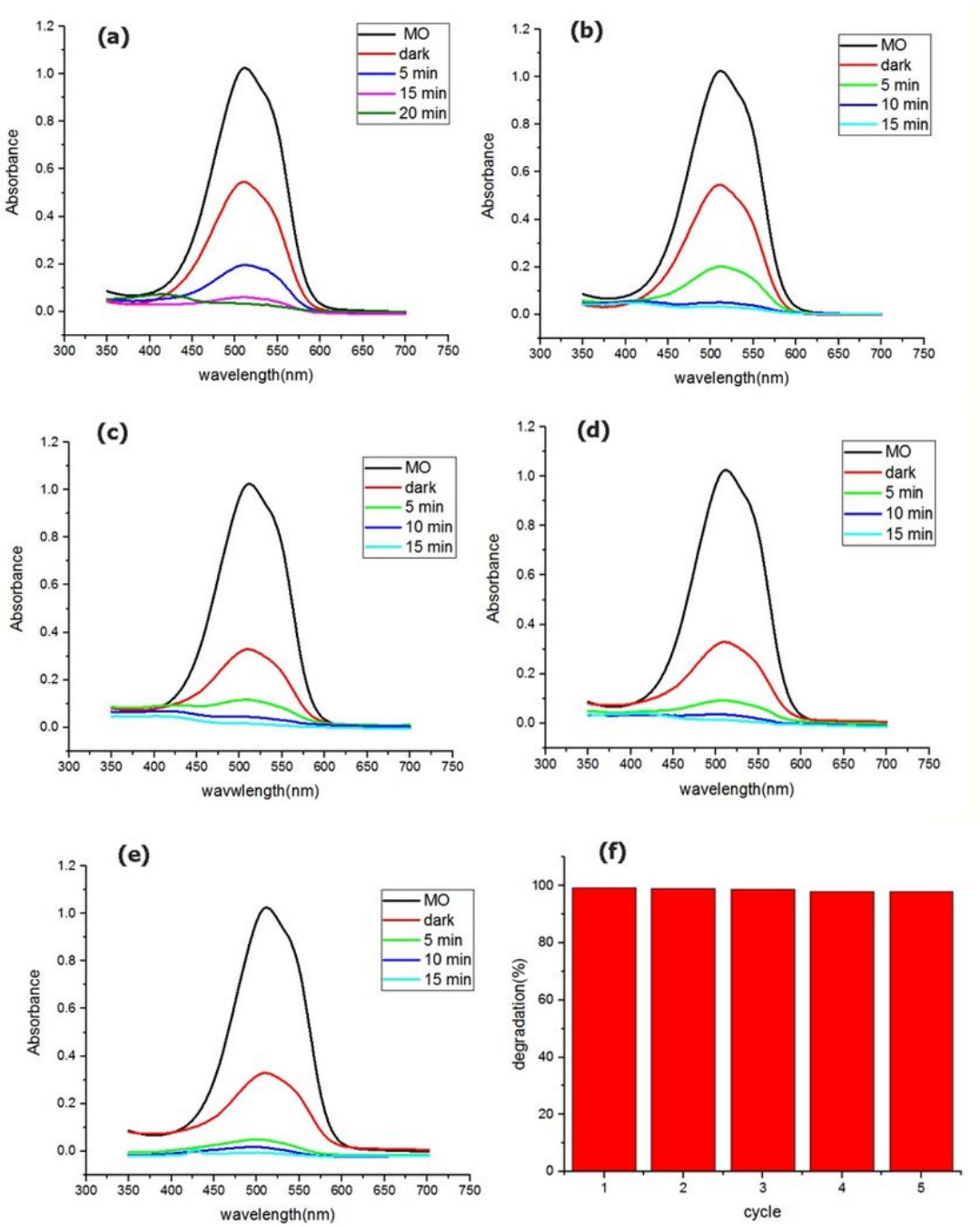

Figure 9

Change in the absorption spectra of methyl orange by CO under (a) UV light and (b) Visible light, Sn-CO under (c) UV light and (d) Visible light, CNT/Sn-CO under (e) Visible light; (f) Cycling runs of MO decolourisation by CNT/Sn-CO samples.

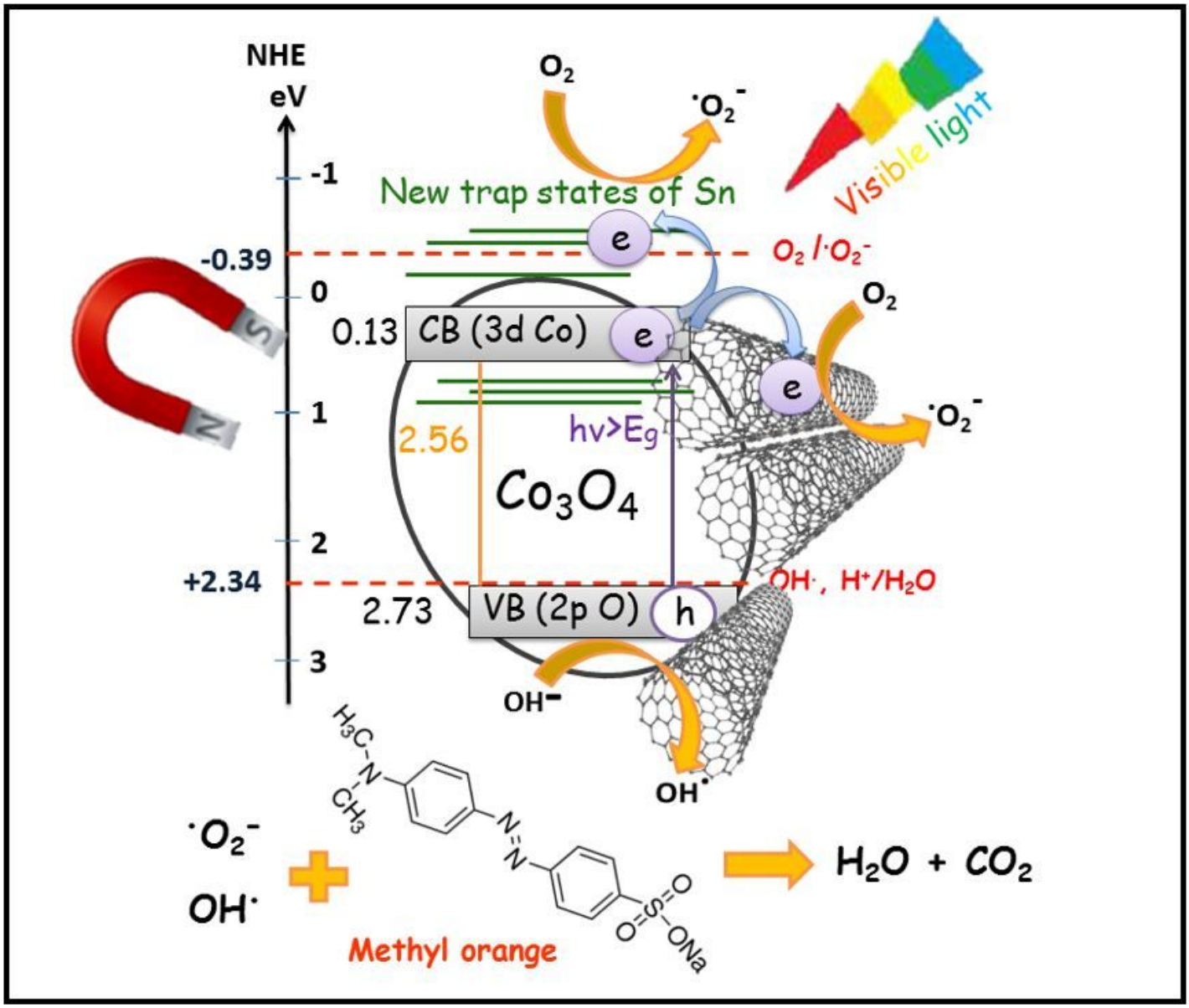

Figure 10

A model for the photocatalytic mechanism of CNT/Sn-CO nanocomposite.